UNIVERSITY OF CAMBRIDGE
Department of Engineering

The interaction between water waves and porous coastlines

Author Name: Micheala Chan
Supervisor: Dr Dongfang Liang

Date: May 28, 2019

I hereby declare that, except where specifically indicated, the work submitted herein is my own original work.

Signed: ______________________________ Date: _______________

Technical abstract

Name: Micheala Ka Yan Chan
College: Trinity Hall
Project title: The interaction between water waves and porous coastlines

Water waves can easily become hydrological or meteorological disasters, causing a threat to human life or resulting in significant economic damage. These problems will only become more significant in the future as climate change causes sea levels and ocean temperatures to rise, thus driving up the frequency and severity of extreme coastal weather events. As such, this project aims to investigate the effect of water-waves on porous media to improve the evaluations of such interactions that can be conducted when designing coastal flood defences.

This report takes a journey through past research conducted in this area (from frictional dissipation of wave energy to wave interactions with porous media to wave impacts), then an explanation of the reasoning behind the methodology used for the project. Following this, the report shows the validation of the material point method (MPM) used to simulate liquid dam-breaks, which form the basis of further simulations of a vertical porous seawall and sloped beach. The porous sloped beach case is investigated further using a wave-generator.

MPM is a numerical technique used to simulate the behaviour of both solids and fluids simultaneously. In MPM, a continuum is broken into two frames: the material points (at which the mass and constitutive equations are solved) and the computational mesh (the nodes of which form the location of the solution of the momentum equations). As a particle-based computational method, MPM has many advantages over traditional mesh-based methods, and has proven itself as highly useful in the field of geotechnical engineering in modelling large deformations and dealing with moving boundary conditions - a key requirement when investigating the relationship between water and soil at the coast.

A basic liquid dam-break is set up in order to validate the MPM code that is being used. It is found that the MPM agrees well with previously validated numerical and experimental data, both in terms of the front propagation of dam-break flows and also in the prediction of pressure distributions. As such, MPM is decided on as the best method moving forward to investigate the effect of water waves on porous media.

The first porous media introduced is a simple extension of the liquid dam-break in that a vertical porous seawall of varying widths is added at the far end of the computational domain. By varying both the grain size of the soil particles forming the wall and the width of the wall itself, it was found that generally run-up decreases with an increase in grain size. At a large enough grain size, it is found that the run-up levels out to a steady-state. This steady-state run-up decreases as the wall width increases. This is thought to be because there is less interaction between percolating particles and running-up liquid particles. At a small enough grain size, the

run-up for all wall widths is the same as the wall simply acts as a non-porous wall.

Further investigations of a similar vein were carried out on the interactions between a water-wave and a porous sloped beach (on which the porous layer is varied in width). The water wave was generated in one of two ways: the first being a simple liquid dam-break, the second being a paddle acting as a wave generator, programmed through modifying the MPM source code. The former has yielded results which imply similar conclusions to the vertical porous seawall while the latter has yet to yield any definitive conclusions. In the case of the wave generator, it appears that below 2 mm, the grain size has only minute effects on the run-up, with variations of less than 1 cm.

Through these investigations, two method of measuring run-up were used. The first was to measure the flow front position, defined as the "*position of the most front particle with a continuous stream of particles following*". Although this is the most direct method of measuring run-up, it is made very difficult and inaccurate by particle scattering, which is found to occur for the vertical seawall at larger grain sizes and at steep slopes (especially the 90° of the vertical seawall).

To continue this research further in the future, it is advised that further investigation is done for the sloped beach case in order to draw more definitive relationships between run-up, porous layer thickness and grain size. Following this, investigating the effect of the slope of the porous sloped beach would enable a fuller picture to be painted.

Of further interest would be to research the effect of multiple waves, as in a regular sea scenario as opposed to the single wave pertaining to a tsunami. As the literature review highlighted the effects that turbulence could have on numerical computations, it is important that a way is found to account for this in the simulations in order to improve accuracy.

Contents

Nomenclature

Ω	Material domain
ρ	Density kgm^{-3}
σ	Cauchy stress tensor
τ	Shear stress
$\mathbf{a}$	Acceleration
$\mathbf{b}$	Specific body force ms^{-2}
$\mathbf{g}$	Gravitational field strength ms^{-2}
$_0$	Subscript index indicating some reference value
D_p	Grain size
H	Incident solitary wave height at constant depth region
h_0	Water depth at constant depth region
K	Bulk modulus kPa
n	Soil porosity
N_n	Number of nodes
N_p	Number of material points
p	Pressure kPa
R_cr	Difference between nonlinear and linear runup
R_s	Maximum wave runup from linear theory
x_p	Position of material point
FLIP	Fluid Implicit Particle
MP	Material point
MPM	Material Point Method
PIC	Particle-in-cell
R	Wave run-up
RVE	Representative Volume Element
SPH	Smoothed Particle Hydrodynamics

1 | Introduction

This project aimed to apply a numerical model to investigate the interaction of waves with porous media.

Water waves can easily become hydrological or meteorological disasters when substantial wave inundation threatens human life or results in significant economic damage. Coastal flooding occurs when normally dry, low-lying land is flooded by seawater. There are three main paths through which coastal flooding happens:

- **Direct inundation**: the height of the sea exceeds the land elevation.
- **Overtopping of a barrier**: the height of the waves exceeds the height of the barrier (either natural or man-made) and water flows over the top of the barrier to flood the land behind it.
- **Breaching of a barrier**: the barrier (either natural or man-made) is broken down by the impact of waves.

1.1 Coastal flood defences

A seawall is an onshore coastal defence structure with the primary aim of protecting areas of human habitation or conservation from wave action, either because of normal tidal processes, or from extreme events resulting from storm surges.

Seawalls are typically large concrete structures. The simplest design is a vertical seawall built parallel to the coastal. This reinforces the existing coastal profile and reflects most of the wave energy to prevent inundation of the area protected behind the wall.

Porous coastal flood defences can also be implemented. These can range from human-engineered structures, such as rubble mounds, to more natural flood defences, such as sand dunes and vegetation.

Rubble mounds are porous structures that allow water to pass through once wave energy has been dissipated. However, these can be damaged by storm waves and can fail by overtopping of broken waves, or by scour and erosion of the underlying seabed.

Natural flood barriers are much less visually intrusive and have demonstrated extreme effectiveness in flood protection. A report published by the United Nations Environment Program (UNEP) suggested that the Boxing Day tsunami in 2004 caused significantly less damage in the areas protected by natural barriers, such as mangroves, coral reefs or coastal vegetation.

Porosity refers to the amount of pore spaces or open space between soil particles. These pore spaces may be the result of root or insect movement. Porosity can also be affected by soil texture. The work done by Ogolo et al. (2015) shows that there is an inversely proportional relationship between porosity and decreasing grain size [15].

Porous structures have many advantages over impervious structures in terms of acting as a sea-wall. A permeable structure is much more effective in reducing the wave run-up, reducing reflected wave height and eventually in reducing the actual pressures on the wall [19].

Analytical solutions have been developed for structures with very simple geometry, but become challenging if faced with any unevenness of the bed. Analytical solutions on water-wave diffraction are rare enough, and in-situ wave loading is notoriously difficult to predict.

Experimental data has also been collected widely by means of hydraulic models. However, this runs into several issues, the largest of which is the scale effect. In relation to wave impacts particularly, large issues arise from the compressibility of air, which is far less significant in a small-scale model than it is in-situ because the increases in the pressure are much lower. Additionally, most model tests are conducted using fresh water, which tends to hold less entrained air than seawater [2]. Finally, flexibility is a significant limitation, as the set up of the lab equipment is costly and time-consuming thus limiting the range of situations and geometries that can be realistically explored. However, basic physical problems such as the dam-break have been investigated, thereby giving us a basis for validation for computational models.

This project focuses on porous media in coastal flood defences, aiming to describe the effect of a varying porosity on the flood defence mechanism. In order to address a wider range of structures and environments, computational methods will be used, specifically the material point method (MPM). The justification for choosing the MPM code is discussed in Chapter 3.

1.2 The effect of climate change on coastal flooding

Climate change refers to the large-scale change in the statistical distribution of weather patterns over a long period of time. There is significant evidence that we are currently in a era of climate change, which has increased both ocean temperatures and sea levels.

A report released by NOAA in 2017 suggests a possible global mean sea level rise of 0.3 - 2.5 m over this century [14]. This has a significant effect on the design of coastal flood defences. If a structure is to have an 80-year design life, the designer must accommodate an additional 2.5 m allowance of protection *in addition to what has already been designed for*.

A rise in sea temperatures has a direct impact on both the frequency and severity of extreme coastal weather events such typhoons, hurricanes and cyclones. As warmer seas provide more energy to developing storms, we can expect that the subject of this project will become an ever-increasingly relevant topic of discussion.

1.3 Brief introduction to MPM

The material point method is a numerical technique used to simulate the behaviour of both solids and fluids simultaneously. It is derived from the fluid implicit particle (FLIP) method, which was developed to overcome the inherent numerical issues with the early implementation of the particle-in-cell (PIC) method. The FLIP method introduces Lagrangian particles, thus removing the need to discretise the convective term, which is a major source of numerical error in the PIC method [1]. The FLIP method can successfully track discontinuities and model highly distorted flows by virtue of the fact that each particle is attributed all fluid properties, including momentum and energy [23].

Unlike in the FLIP method, the governing equations are presented in the weak formulation in the MPM method. This is consistent with the finite element method (FEM), which has been the dominant computation method used in geotechnical engineering. Another difference between the MPM and FLIP methods is in the invocation of the constitutive equation at the material points in MPM, as opposed to FLIP which solves the constitutive equation at the grid nodes [20].

In MPM, a continuum body is described by small Lagrangian elements referred to as "material points" (MPs). The MPM is categorised as a continuum-based particle method (i.e. meshless), like the smoothed particle hydrodynamics (SPH) method. As such, MPM does not encounter the drawbacks associated with mesh-based methods – namely advection errors and deformation tangling – which makes it a powerful tool in computational geomechanics. Although there is a mesh, it is only used to solve for the governing equations for computational convenience and all properties of the continuum material are assigned to the material points - the mesh does not carry any permanent information.

The MPM code has been recently extended to handle multi-phase problems with a single layer of material points or two layer of material points. Its applications have included seepage flow through embankments, and wave attack on sea dikes.

1.4 Aims

In order to develop safe and efficient coastal protection methods, it is important to conduct detailed analysis into wave run-up and breaking around porous structures. This research aims to apply a numerical model for analysing the interactions between water waves and soil to simulate wave propagation and run-up around porous media. This will be explored through a number of simulations looking at the relationship between grain size, run-up and porous media width, for both vertical seawalls and sloped beaches. It is hoped that this research will contribute to improving the understanding of fluid flow around permeable media, such that better evaluations of wave-structure interactions can be conducted when designing coastal flood defences to deal with increasingly extreme weather events.

2 | Literature review

Initial research into hydrodynamic phenomena was carried out using physical models to determine empirical coefficients and to provide evidence for underlying mathematical theory. Experimental tests can also be conducted in flumes using scale models of coastal defences to validate analytical theory.

2.1 Frictional dissipation of wave energy

Savage and Fairchild (1953) conducted one of the first investigations into frictional dissipation of wave energy by porous media [17]. Using a wave flume with a splitter wall, the wave energy loss by bottom friction and percolation were investigated. Sands were used for the permeable bottom and, under the condition of artificial ripples, the maximum energy loss reached 60 percent. Although the maximum frictional loss agreed well with theoretical values, the percolation loss values required correction factors of 4 to 10 to obtain reasonable agreement with the theory. Losses for low-permeability sands were insignificant though large percolation losses were found when sand sizes larger than 2 mm were used. This demonstrates that porous media can be effective at dissipating wave energy, but the amount of energy dissipated is dependent on the material porosity.

2.2 Wave interaction with porous media

Straub et al. (1957) were amongst the first to study wave interactions with porous media. The study found that a material with a high porosity was desirable, and that crushed rock laid or packed to produce a high enough porosity was almost as effective as metal meshes on low surface slopes [18].

Lean (1967) investigated the reflection of waves from simple permeable wave absorbers and found that some reflection will always occur [8].

Sulisz (1985) formulated a theory that predicts wave reflection and transmission at an infinite rubble-mound breakwater if the incident wave meets the structure from a normal direction. This showed a reasonable agreement with experimental results [19].

Huang and Chao (1992) investigated a small-amplitude water wave acting on a vertical porous breakwater in an infinitely long channel. Homogeneous water follows conventional assumptions as irrotational, inviscid, incompressible fluid flow. The porous breakwater has a rigid solid skeleton and the flow inside the porous breakwater is governed by simplified Biot theory of poroelasticity. A small "porous Reynolds number" was applied to obtain a regular perturbation solution that preserves the surface of seepage on the breakwater/channel flow interface. They observed that there are dramatic variations of velocity distributions among vertical cross-sections inside the porous breakwater. They identified that the reflected wave is greater, while the transmitted wave is less for higher frequency waves with thicker and less porous breakwaters. The thickness of the porous breakwater only has a significant effect on the transmitted wave [6].

Liu et al. (1999) presents a numerical model for simulating wave interaction with porous structures [12]. The paper combined the free surface-capturing approach together with a novel Cartesian cut cell treatment. The Finite Volume Model calculates the two-phase flows outside porous structure based on the Navier-Stokes equations; the Navier-Stokes type model equations describe the flow in the porous structure. The numerical model is used to be simulate the breaking wave overtopping a caisson breakwater, which is protected by a layer of armour units. The results show that the porous armour layer is effective in reducing the overtopping of the caisson breakwater.

Sakakiyama and Liu (2001) focused experimentally on wave behaviour and turbulence flows in front of a caisson breakwater, which was covered with wave-absorbing blocks and supported by a rubble mound. They concluded that turbulence is generated around the caisson breakwater during a wave breaking process, which significantly affects wave impacts and the scouring process in front of the breakwater [16].

Koraim et al. (2014) investigated the hydrodynamic efficiency of a new type of porous seawall experimentally. The observed that the run-up and reflection coefficients decrease with increasing porosity: increasing seawall porosity from n = 0.38 to 0.47 decreases the wave run-up and reflection coefficients by 5-10% [7].

2.3 Wave impact

Impact pressures on coastal structures are generated by all types of breaking waves. It is generally known that a wave breaking directly onto a wall will produce much greater impact pressures than a non-breaking wave. Thus, impact pressures are highly relevant to the design of coastal flood defences.

Hattori et al. (1994) performed experiments for wave impact on vertical walls under breaking waves. The experiments found that when a small bubble of air is trapped between a breaking wave and the wall at collision, the impact pressure increases considerably - this is when the highest pressure occurs [4]. Bullock et al. (2007) carried out a detailed investigation into the characteristic of wave impacts against both vertical and inclined walls [2]. They found that the most substantial impact pressures occur at the stillwater level. They also observed that nominally identical waves may produce very different pressure distributions, but similar impulses - the impulse on a structure during impact is shown to be broadly proportional to the peak momentum flux of the incident waves.

2.4 Summary

Since the 1950s, the understanding of wave motion and impact has significantly improved. However, only a few analytical models have been developed and validated whilst many physical experiments have been conducted. The major difficulties with laboratory experiments outlined above include scaling effects and also flexibility of planning and use.

Recently research has tended to use laboratory experiments to investigate basic physical problems, such as the simple dam-breaking and solitary wave propagation scenarios. These results can be used to validate simulations and numerical models, which can then be used to carry out more complex investigations.

3 | Methodology

3.1 MPM

Many engineering problems can cause severe numerical problems in computational models. In the case of failures of man-made structures and natural hazards arising from gravity-driven flows (such as landslides, dam-breaks) constitutive equations are history dependent so material points must be followed.

The material point method uses a continuum based on soil constitutive models, most typically the Mohr-Coulomb, Cam Clay or Modified Cam Clay models; instead of grains, the material points are viewed as representative volume elements (RVE). In MPM, the computational domain is spatially discretised in two frames, as shown in Figure 3.1. First, the continuum body is divided into a group of MPs. Each particle carries all the material variables: mass, velocity, stress, strain and position. This characteristic makes the MPM convenient for modelling based on history-dependent constitutive material points. Each point also has a constant mass (thus automatically fulfilling mass conservation) but has a volume which can change, thereby enabling material compression or extension. Each MP moves with the body's deformation. The mass and constitutive equations are solved at the MPs.

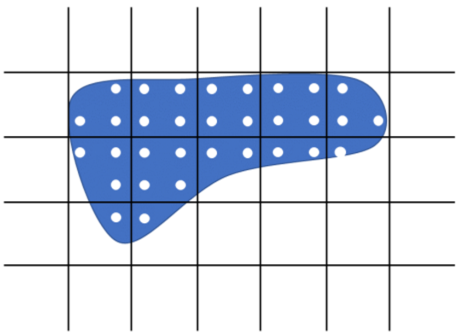

Figure 3.1: Spatial discretisation of a continuum body

The second frame is the computational mesh, equivalent to a conventional finite element mesh, and covers the full domain of the problem - including any empty space in which particles may have to move into. The momentum equations are solved at the nodes of this computational mesh. The variables required to solve the governing equations for each step of the calculation are transferred from the material points to the nodes of the mesh using mapping functions. Boundary conditions are imposed, either at the mesh nodes or at the MPs, and an incremental scheme is used to solve the governing equations. The quantities carried by the MPs are updated through the interpolation of the mesh results, using the same mapping functions. The information associated with the mesh can be discarded to avoid any mesh distortion, as it is not needed for the next step of the analysis.

In MPM, as it is the particle and not the mesh points that store all the information on the state of the calculation, no numerical error results from the mesh returning to its original position after each step and no re-meshing is required. Once the momentum balance equation is solved at each node of the background mesh and the location of the material points has been updated, the background mesh is reset to the original position, as depicted in Figure 3.2.

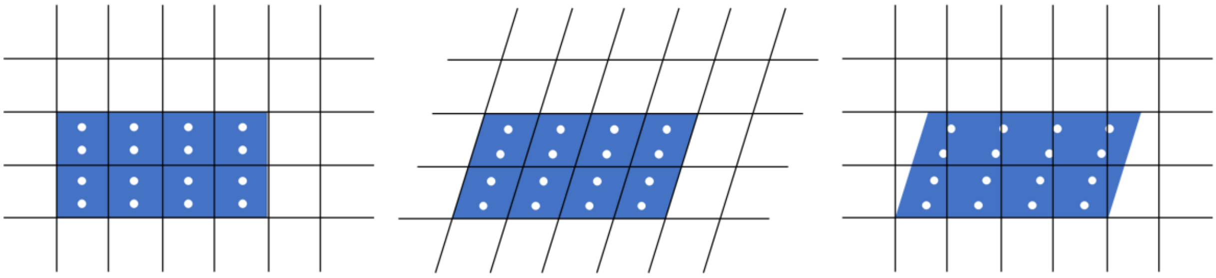
(a) (b) (c)

Figure 3.2: Material points and a background mesh at: (a) the initial position. (b) during the intermediate time step. (c) the updated position

Following material points is difficult to implement in an Eulerian scheme. However, modelling using purely Lagrangian methods typically results in severe mesh distortion, leading to mesh lock-up or entanglement. In MPM, mesh tangling is avoided since the fixed Eulerian grid can be interpreted as an updated Lagrangian frame of reference and so the usual convection term in the acceleration associated with Eulerian formulations does not appear [20].

MPM has proven to be useful in modelling large deformations and dealing with moving boundary conditions. In addition to this, it has several advantages over the next best particle (mesh-free) method - SPH, in which a continuum material is divided into a set of particles. Each particle is assigned a spatial distance called a smoothing length in which the physical properties of each particle is smoothed using a kernel function. Although both MPM and SPH show more promising results than mesh-based methods, SPH encounters many problems involving boundary interfaces (such as the soil-water interface), particularly a reduction in accuracy near boundaries since insufficient neighbouring particles result in a loss of consistency. Since two-phase MPM is more widely researched than two-phase SPH and the fact that the soil-water interaction is critical in this project, MPM has been chosen as the most suitable method for studying water-wave interaction with porous media.

3.2 Governing equations

The basis for the theoretical understanding of dam-break flows is provided by shallow water theory. Discontinuities in the weak form of the solution can be used to represent shocks in the flow since the shallow water equations

In order to obtain the shallow water equations, we must integrate over depth from the three-dimensional Navier-Stokes equations. Although the formulation of the shallow water equations is not explored here, these equations are often favoured in flood situations as their description is both convenient and accurate for almost horizontal flows [22].

The material domain Ω is represented by a number of material points N_p and the position of the material point at the current instant (time t) is denoted by x_p. The same material point at the initial time (t = 0) is denoted x_p^0. The governing equations describing the continuum body are the standard conservation equations: mass (Equation 3.1) and momentum (Equation 3.2).

$$\frac{\partial \rho}{\partial t} + \rho \Delta \cdot \nu = 0 \tag{3.1}$$

$$\rho \mathbf{a} = \Delta \cdot \sigma + \rho \mathbf{b} \tag{3.2}$$

where $\rho(\mathbf{x}, t)$ is the density of the continuum body, acceleration $\mathbf{a}(\mathbf{x}, t)$ is the material derivative of the velocity $\mathbf{v}(\mathbf{x}, t)$, $\mathbf{b}$ is a specific body force and σ is the Cauchy stress tensor that can be decomposed into pressure and deviatoric components. The water pressure is linked to its density change:

$$p = p_0 + K\frac{\rho}{\rho_0} \tag{3.3}$$

where K is the bulk modulus of water, p is pressure, and the subscript indicate an initial reference value.

In the MPM, the Langrangian framework removes the need for a non-linear convective term. The positions of each material point are updated with every timestep.

3.3 Weak form of the governing equations

Each material point carries the field variables, mass M_p, density $\rho(\mathbf{x}, t)$, velocity $\mathbf{v}_p(\mathbf{x}, t)$ and the Cauchy stress $\sigma(\mathbf{x}, t)$, for p = 1, 2, 3...N_p. Since the mass M_p is constant throughout the computation, the mass is automatically conserved in MPM.

At the current instant, the density of the continuum body can be expressed as:

$$\rho(\mathbf{x}, t) = \sum_{p=1}^{N_p} M_p \delta(\mathbf{x} - \mathbf{x}_p) \tag{3.4}$$

where $\delta()$ is the Dirac delta function. This leads to the following relationship:

$$\int \rho dV = \sum M_p \delta(\mathbf{x} - \mathbf{x}_p) dV \tag{3.5}$$

The weak form of the momentum equation can then be formed by multiplying the equation of conservation of momentum by a test function $\mathbf{w}$:

$$\int_\Omega (\rho \mathbf{w} - \mathbf{w}\Delta \cdot \sigma - \rho \mathbf{w} \cdot \mathbf{b}) dV = 0 \tag{3.6}$$

Applying the divergence theorem to Equation 3.6 allows us to write the weak form of the momentum equations as:

$$\int_\Omega \rho \mathbf{w} \cdot \mathbf{a} dV = -\int_\Omega \sigma : \Delta \mathbf{w} dV + \int_\Omega \rho \mathbf{w} \cdot \mathbf{b} dV + \int_{\partial\Omega} \mathbf{w} \cdot \tau dS \tag{3.7}$$

Let $M_p = \int \rho dV$, we can approximate Equation 3.7 by a summation of quantities at material points:

$$\begin{aligned}
\sum_{p=1}^{N_p} M_p \mathbf{w}(\mathbf{x}_p, t) \cdot \mathbf{a}(\mathbf{x}_p, t) = \; & -\sum_{p=1}^{N_p} M_p \sigma^s(\mathbf{x}_p, t) : \mathbf{w}(\mathbf{x}, t)|_{\mathbf{x}=\mathbf{x}_p} \\
& + \sum_{p=1}^{N_p} M_p \mathbf{w}(\mathbf{x}_p, t) \cdot \mathbf{b}(\mathbf{x}_p, t) \\
& + \int_{\partial\Omega} \mathbf{w} \cdot \tau dS
\end{aligned} \tag{3.8}$$

where σ^s is a specific stress.

3.4 Discretisation

If we consider an Eulerian grid with a total number of nodes N_n, standard nodal basis functions, $N_i(\mathbf{x})$ with i = 1 – N_n can be defined in the same way as in standard FEM. Rewriting the acceleration $\mathbf{a}(\mathbf{x}, t)$ and test function $\mathbf{w}(\mathbf{x}_p, t)$ at material point $\mathbf{x}_p$ in terms of nodal basis functions gives the following equations:

$$\begin{aligned}
\mathbf{a} &= \sum_{i=1}^{N_n} \mathbf{a}_i(t) N_i(\mathbf{x}) \\
\mathbf{w} &= \sum_{i=1}^{N_n} \mathbf{w}_i(t) N_i(\mathbf{x})
\end{aligned} \tag{3.9}$$

We can substitute these to Equation 3.7, resulting in a discretised equation:

$$\sum_{i=1}^{N_n} \mathbf{w}_i \cdot \sum_{j=1}^{N_n} m_{ij} \mathbf{a}_j = -\sum_{i=1}^{N_n} \mathbf{w}_i \cdot \sum_{p=1}^{N_p} M_p \sigma_p^s \cdot \Delta N_i(\mathbf{x})|_{\mathbf{x}=\mathbf{x}_p} + \sum_{i=1}^{N_n} \mathbf{w}_i \cdot \mathbf{b}_i + \sum_{i=1}^{N_n} \mathbf{w}_i \cdot \tau_i \tag{3.10}$$

where the mass matrix m_{ij} is defined as:

$$m_{ij} = \sum_{p=1}^{N_n} M_p N_i(\mathbf{x}_p) N_j(\mathbf{x}_p) \tag{3.11}$$

The applied traction, τ_i is:

$$\tau_i = \int_{\partial\Omega} \tau(\mathbf{x}, t) N_i(\mathbf{x}) dS \tag{3.12}$$

and the specific body force, $\mathbf{b}_i$ is:

$$\mathbf{b}_i = \sum_{p=1}^{N_n} (\mathbf{x}, t) N_i(\mathbf{x}_p) \tag{3.13}$$

Then, considering the arbitrary nature of $\mathbf{w}_i$, we can rewrite Equation 3.10 in a reduced form. From this we can solve for the acceleration $\mathbf{a}$ at the grid nodes by solving N_n coupled linear equations.

$$\sum_{j=1}^{N_n} m_{ij} \mathbf{a}_j = \mathbf{f}_i^{int} + \mathbf{f}_i^{ext} \tag{3.14}$$

where

$$\mathbf{f}_i^{int} = -\sum_{p=1}^{N_p} M_p \Delta N_i(\mathbf{x})|_{\mathbf{x}=\mathbf{x}_p} \cdot \sigma_p^s \tag{3.15}$$

$$\mathbf{f}_i^{ext} = \mathbf{b}_i + \tau_i \tag{3.16}$$

3.5 Two-phase formulation

MPM can deal with soil and liquid simultaneously. To allow for this, the solid and liquid phases are assigned separate sets of material points, such that saturated soil can be regarded as soil particles floating within a fluid or a porous medium surrounded by liquid. The momentum balance equations for the MP layers are presented by separate velocity fields as follows:

$$\Delta \cdot \sigma_s' + n_s \Delta \cdot \sigma_l + \bar{\rho}_s \mathbf{g} + \mathbf{f}_d = \bar{\rho}_s \frac{du_s}{dt} \tag{3.17}$$

$$n_l \Delta \cdot \sigma_l + \bar{\rho}_l \mathbf{g} - \mathbf{f}_d = \bar{\rho}_s \frac{du_l}{dt} \tag{3.18}$$

where the subscripts *s* and *l* denote the solid and liquid respectively, $\bar{\rho}$ is the partial density, *n* is the concentration ratio defined as the ratio of the partial density $\bar{\rho}$ to the corresponding mass density. $\mathbf{f}_d$ is the drag force exerted by the liquid on the soil.

When two sets of material points are used, the mixture must be identified by its *state*, characterised by the dominant material.

3.6 Numerical implementation

During the course of the MPM computation, the unknown variables are always recorded by the material points, but are interpolated onto the grid at the beginning of each time step. In order to eliminate divisions by nodal masses, momentum is used in place of velocity as much as possible in the code. Further, the velocity gradient used to calculate the strain rate at material points is calculated using the updated particle velocities mapped onto the grid nodes [21].

The general computation procedure in each time step is as follows:

1. Initialise the grid and material points.
2. Extrapolate material point quantities to grid nodes.
3. Solve equations of motion on the grid.
4. Solve Equation 3.14 to obtain the nodal acceleration.
5. Extrapolate derivative terms back to the material points.
6. Grid is reset and material point positions is updated.

3.7 Anura3D

The Anura3D MPM Software is being developed by the Anura3D MPM Research Community. The research community is a collaboration of a number of university research groups who have developed a software tool for MPM analyses of geotechnical problems which uses a 3D implementation of the material point method.

4 | MPM simulations: Verification

The MPM code that was used for these simulations was developed by the Anura3D MPM Research Community (http://mpm-dredge.eu).

The domain is meshed with structured tetrahedral elements and used to initialise the material points. Finer meshes with smaller cells initialise more material points, which individually have smaller masses compared to those larger once generated by coarser meshes. For simple simulations, the mesh is a regular structured mesh.

The first simulation run was a dam-break within a non-porous domain. The idealised dam-break collapse problem is a classical problem which is often run to validate a numerical mode, due to its simple initial and boundary conditions. In this report, the collapse of a water column and a granular column are simulated separately. It is found that a liquid flow will tend to form a single wave, whereas a granular column will fail, crumble and flow to form a deposition on the flat bottom surface.

Figure 4.1 shows a sketch of the idealised dam-break problem. The initial height of the column is 2 m, and the width is 1 m. These dimensions match those used in Fern and Soga (2016) [3] and Zhao et al. (2017) [23]. The walls and the bottom surface are all impermeable. A "slip" condition is applied on the bottom boundary to allow flow along the bed.

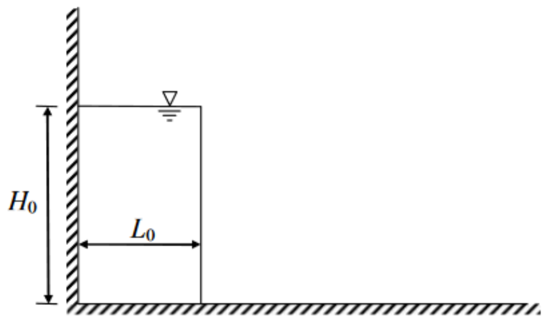

Figure 4.1: Sketch of the idealised dam-break in a tank from Zhao et al. (2017)

4.1 Granular flows

4.1.1 Definition of geometry and mesh

The initial geometry is shown in Figure 4.2, with parameter values as given in Table 4.1. The calculation is performed in two stages:

1. initialisation of stresses by quasi-static gravity loading
2. failure of the column by removal of column fixities

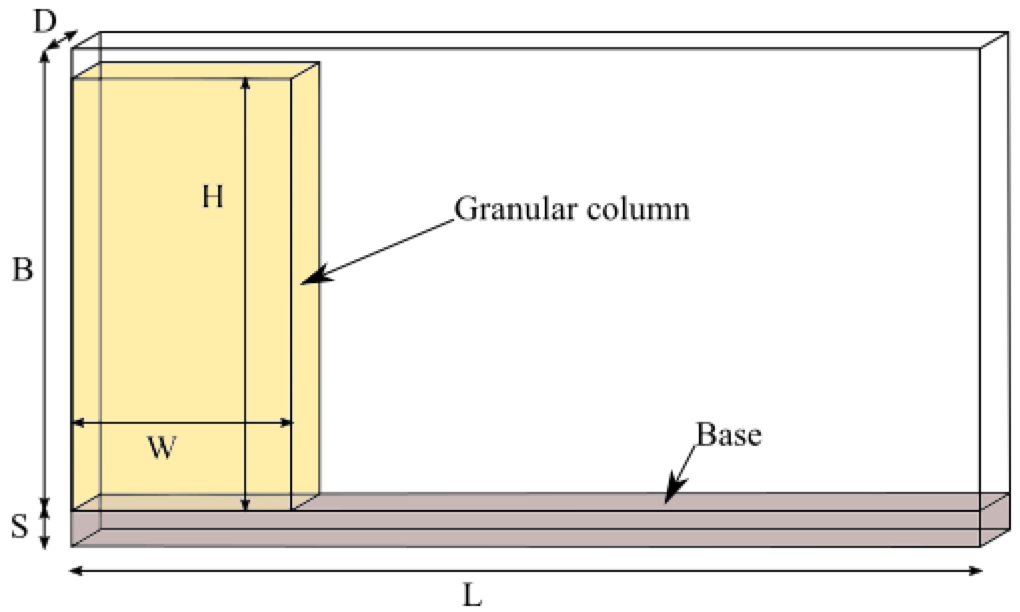

Figure 4.2: Initial geometry for the dam break, including a base layer used for the granular case

4.1.2 Boundary conditions

Boundary conditions are represented by *fixities* in MPM. If a boundary surface is fixed with a certain fixity, material points of the type defined cannot penetrate that surface. In this simulation, the right, left and bottom sides of the flume are fixed to prevent material points from leaving the computational domain. The right column boundary is fixed whilst the stresses are initialised; it is then removed to simulate the dam breaking. The boundary conditions are only applied for the solid phase as this is a one phase calculation.

4.1.3 Parameters

The number of material points was changed along in order to ensure consistency in simulation resolution. Fern and Soga (2016) found, through a mesh sensitivity analysis, that increasing the number of material points in a coarse mesh did not significantly improve results [3]. However it was found that refining the mesh significantly improves the results. This is because more material points are initialised. A fine mesh produces a convex failure surface via a process called avalanching which is mesh dependent, while a coarse mesh results in a concave failure surface [3].

Table 4.1: Granular simulation parameters

Ratio α	Height H (m)	Width W (m)	Depth D (m)	Box height B (m)	Box width L (m)	Base S (m)	Mesh size (m)	MPs #
2	2	1	0.1	2.2	5	0.2	0.1	8

4.1.4 Material properties

The material properties for the granular simulations are shown in Table 4.2.

Table 4.2: Material properties for granular simulations

material	**column**	**base**
material type	dry material	dry material
material model	Mohr-Coulomb	Linear elasticity
initial porosity	0.4	0.4
density [kg/m^3]	2650	2650
K_0 value [–]	0.0	0.0
Young's modulus, E [kPa]	10	10
Poisson's ratio [–]	0.2	0.3
cohesion [kPa]	0	-
friction angle [°]	33	-
dilatancy angle [°]	0	0
tensile strength [kPa]	0	0

4.1.5 Results

The total displacements, deviatoric strain and vertical effective stress after collapse are shown in Figure 4.3 for the case where α = 2.

Verification

The primary failure surface and final depositions from the granular column collapse were compared with those in Fern et al. (2016) [3]. Figure 4.4 shows the comparison for aspect ratio α = 2.

The overall shape shows good agreement. However, in the final deposition, the Fern et al. (2016) simulations show a greater run-out distance and a more convex failure plane. This may be due to the simulation resolution. The number of material points affects run-out distance - the effect of mesh coarseness on failure plane shape has been discussed briefly in 4.1.3. Increasing the resolution would improve the results, but would come at an increased computational cost.

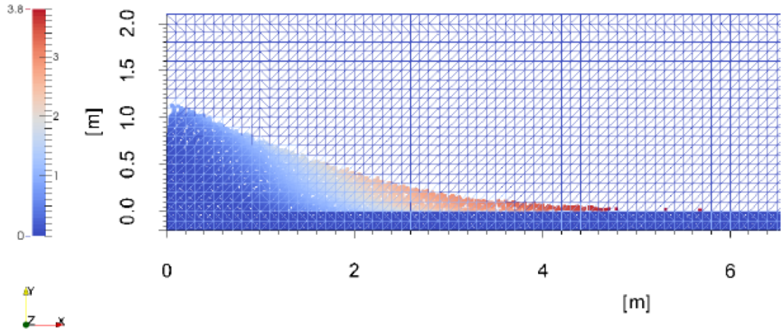

(a)

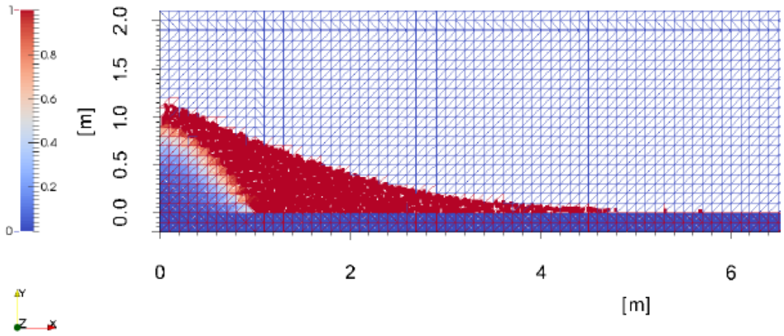

(b)

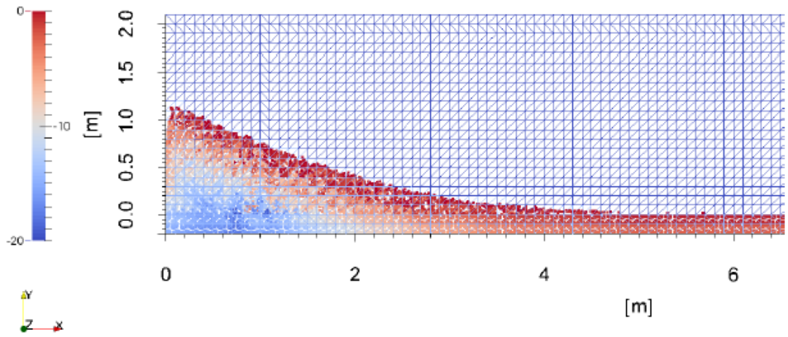

(c)

Figure 4.3: Results after collapse for one-phase dry soil for α = 2: (a) Total displacement (m). (b) Deviatoric strain. (c) Vertical effective stress (kPa)

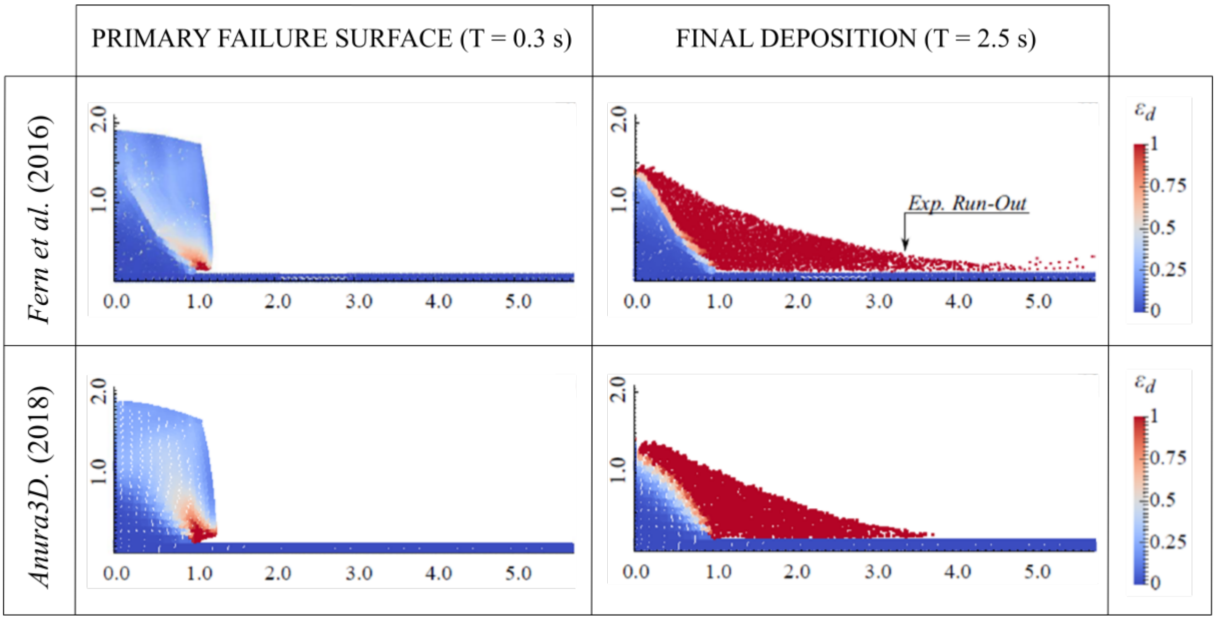

Figure 4.4: Verification of granular simulation for α = 2, all distances in metres

4.2 Liquid dam-break flows

This case is the MPM model that will form the basis of the investigation into water-wave impact on porous media and is first validated through a comparison of a liquid dam-break flow against existing experimental and numerical data.

Viscous and turbulent effects are not considered in dam-break floods whose behaviours are All surfaces are assumed to be frictionless.

4.2.1 Definition of geometry and mesh

The initial geometry is shown in Figure 4.5. As Anura3D 2018.1 does not allow liquid and solid material to be simulated together, the base layer must be removed, leaving only the column and the non-porous domain.

4.2.2 Boundary conditions

In this simulation, the right, left and bottom surfaces of the flume are fixed to prevent movement of material points outside of the computational domain. In the liquid case, slip is allowed on the bottom boundary. Additionally there is no need to remove fixities as the initialisation of stresses in the first step is carried out using the K0 procedure (the liquid is hydrostatic).

4.2.3 Parameters

The number of material points and the size of the domain was changed to ensure consistency in simulation resolution. The dam-break simulation's dependency on the computation mesh size

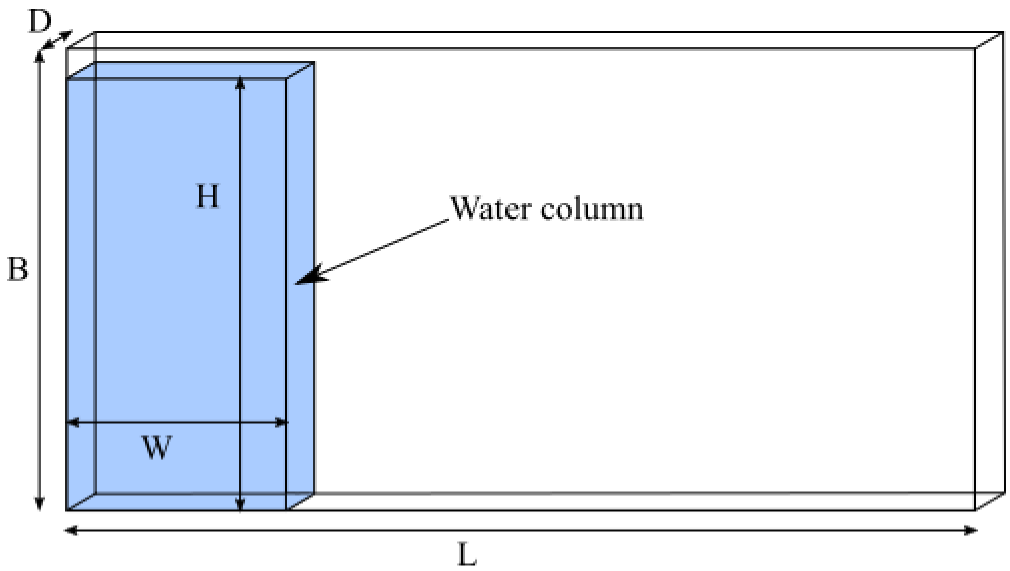

Figure 4.5: Initial geometry for the liquid case

and particle density were investigated in Zhao et al. (2017), which found that the mesh size and particle density do not play an important role in the results of dam-break simulations. [23]

Table 4.3: Liquid simulation parameters

Ratio α	Height H (m)	Width W (m)	Depth D (m)	Box height B (m)	Box width L (m)	Mesh size (m)	MPs #
2	2	1	0.1	2.2	5	0.1	8

4.2.4 Material properties

The material properties for the liquid simulations are shown in Table 4.4. To achieve a relatively large time step, an unrealistically low bulk modulus of water was chosen, as in Zhao et al. (2017) [23]. This results in increased compressibility, which does not affect the simulation if the speed of the modelled water is over ten times larger than the maximum flow speed across the domain [11].

Table 4.4: Material properties for liquid simulations

material	**water**
material type	liquid
bulk modulus [kPa]	20000
dynamic viscosity [kPa/s]	1e-06
density, ρ [kg/m^3]	1000
liquid cavitation [kPa]	0
detect free surface	yes

4.2.5 Results

The results for the liquid column collapse for the case of aspect ratio α = 2 are shown in Figure 4.6.

Validation

The results obtained for the liquid dam-break flow with aspect ratio α = 2 are compared with the validated results presented in Liang (2010) [11], where the column collapse is modelled using SPH, and in Zhao et al. (2017) [23], in which the column collapse is modelled in MPM. The water surface profiles predicted by the shallow water equations (SWE) are indicated by the solid line on the MPM plots in the second column. These results are shown in Figure 4.7.

The Anura3D code, whilst predicting accurate water surface profiles, predicts pore pressure inaccurately. The MPM code, however, shows excellent agreement in both the shape and the pore pressures. The results for the liquid case are thus taken from simulations using the MPM code.

Parametric study

To compare the results across different aspect ratios, distance and time have been scaled according to the Froude law:

$$t^* = \frac{t}{\sqrt{\frac{H_0}{\mathbf{g}}}} \qquad x^* = \frac{x}{H_0} \tag{4.1}$$

where t^* is the normalised time, x^* is the normalised position of the flood front, *t* is time, *x* is the position of the flood front, H_0 is the initial height of the water column and g is the gravitational acceleration.

A quantitative comparison of the position of the flood front in the MPM simulations is compared to published results for SPH [11], Volume-of-Fluid (VOF) method [5], and SWEs [11] and experimental data [13] is shown in Figure 4.8. The flow front position is defined as the "*position of the most front particle with a continuous stream of particles following*" [23]. Any small dispersed particles leading the flow are ignored. However, as front positions are obtained by visual identification, there is potential for errors to be introduced.

The MPM simulations appear to agree well with previously verified MPM simulations, as well as with both the experimental data and the previously published numerical results. The Anura3D results are also similar and are the closest to the SPH simulations. The SWEs solver tends to overestimate the propagation speed as it assumes negligible vertical momentum and is therefore not considered in this analysis.

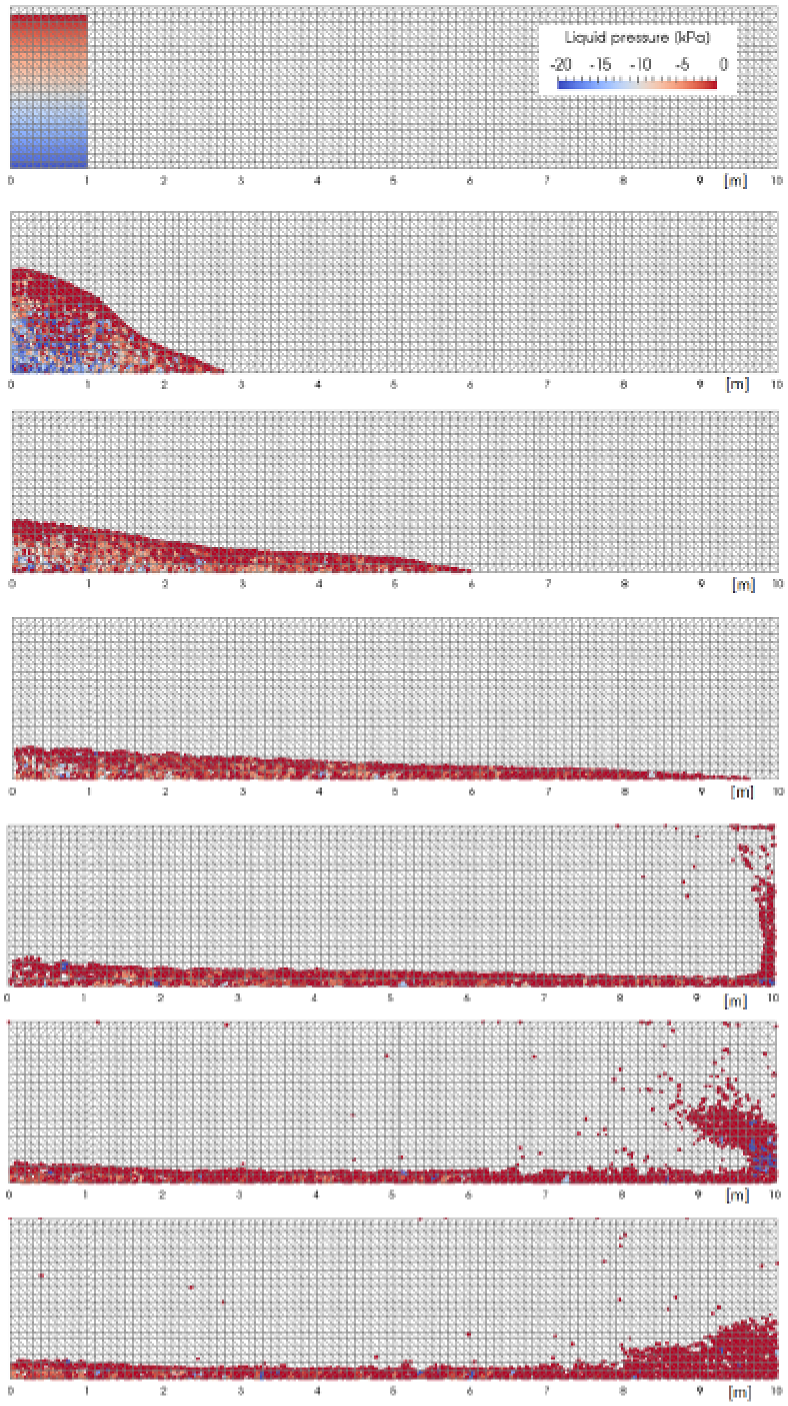

Figure 4.6: Results of a liquid column collapse for α = 2 from t = 0 to t = 0.7s

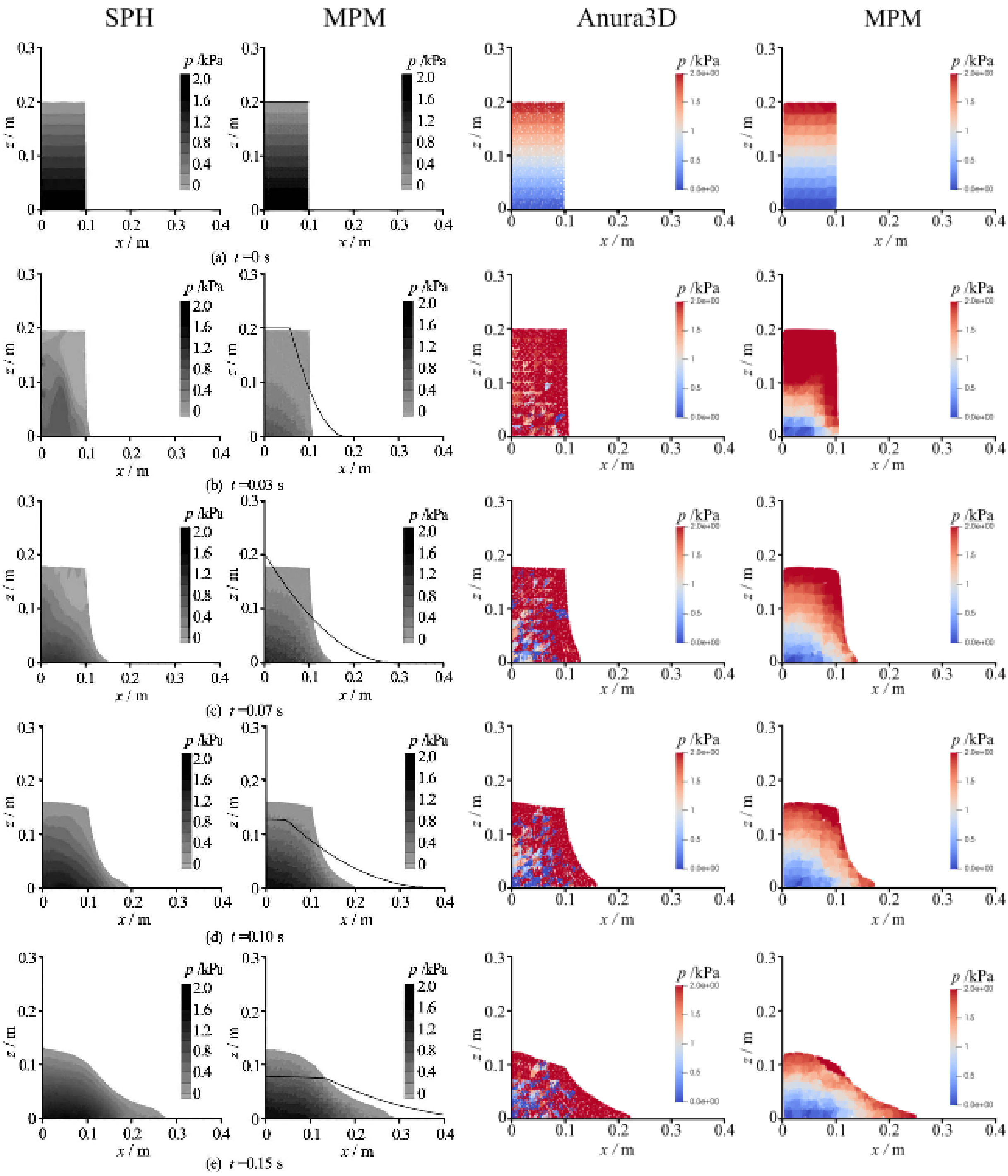

Figure 4.7: Comparison of the results produced by Liang in SPH and by Zhao in MPM (left) with the results produced by the Anura3D (right)

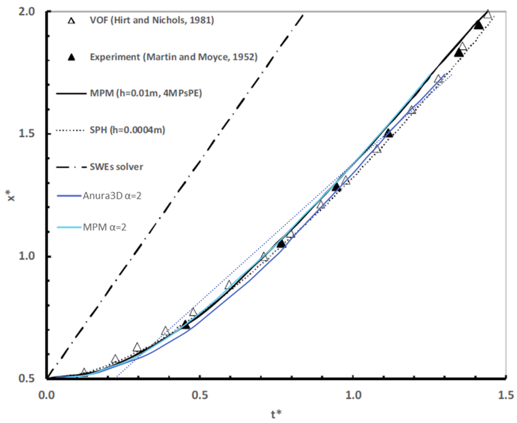

Figure 4.8: Change in flood front position with time

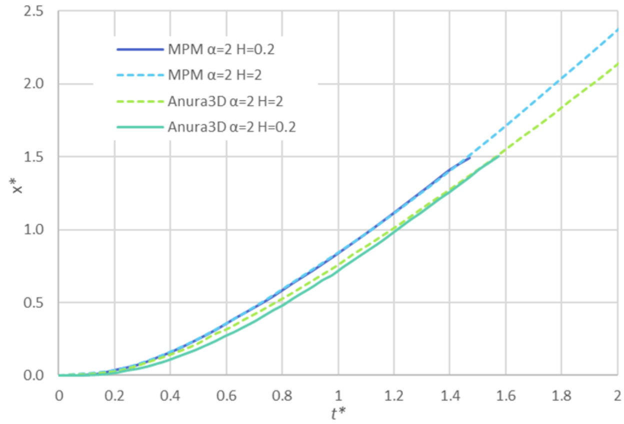

Figure 4.9: Comparison of different scales in Anura3D and MPM at $\alpha = 2$

Keeping the same aspect ratio, the initial parameters do not affect the results as they are non-dimensionalised. This can be seen in Figure 4.9, which compares simulations to those at $\frac{1}{10}$ scale.

4.3 Discussion

The MPM code has demonstrated results concurrent with published results. Compared with other verified numerical simulations and experimental data, the MPM simulations give good predictions of the pressure distribution and the front propagation of dam-break flows. The mesh size and number of material points has little effect on the results for the liquid case.

From these simulations, it was decided that it was possible to use the MPM to model dam-break flows and to generate a water wave to investigate interaction with a porous medium of changing porosity and width.

5 | Porous Seawall

This chapter describes the effect of changing the permeability of a porous barrier on the run-up height, by way of changing the soil grain size. The wall width is also varied to explore whether it has a significant impact on the run-up height. These simulations use the Anura3D double-point MPM code. A Courant number of 0.8 is used to ensure stability.

5.1 Definition of geometry and mesh

The initial geometry used for this case is shown in Figure 5.1. The porous seawall is represented by a vertical rectangular porous wall, with the 'wave' based on the liquid dam-break flow as explored earlier. The wall width takes the values of $[0.1, 0.2, 0.3, 0.5]$ m. The height B is set so that the run-up generated by the incoming water never reaches the top of the domain, as the reflection of liquid particles from the top of the domain would affect the run-up. The thickness of the domain is one mesh unit wide. The liquid column has 20 fluid material points specified per element, and the soil column has 4 solid material points specified per element.

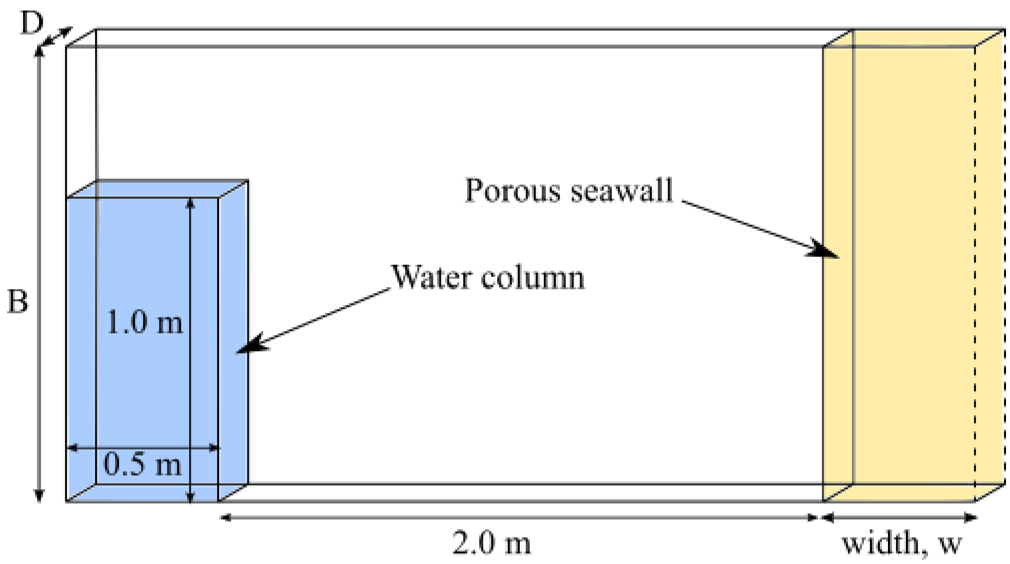

Figure 5.1: Initial geometry for the porous seawall case

5.2 Boundary conditions

In this simulation, the surfaces on the right, left and bottom surfaces are fixed to prevent material points leaving the domain. A solid fixity is also used on the left side of the porous seawall to prevent its collapse. There is no liquid fixity applied to this side in order to allow the liquid particles to flow into the porous medium.

5.3 Material properties

Table 5.1 shows the material properties of the elastic soil used for the porous seawall. The properties of the liquid water column are as shown in Table 4.4. The grain size was varied between 1 mm and 0.15 m. The maximum allowable porosity in these simulations is 0.7. This parameter distinguishes the solid and liquid states and must be at least as large as the initial porosity of the soil lest the soil liquefies when the simulation begins. The porosity of the soil is not changed in these simulations - the permeability of the material is only altered through variations of the material.

Table 5.1: Material properties for porous seawall

material	**elastic soil**
material type	dry material
material model	Linear elasticity
initial porosity	0.43
density, ρ [kg/m^3]	2650
K_0 value	0
Intrinsic permeability [m^2]	1e-09
Young's modulus, E [MPa]	10
Poisson's ratio	0.3

5.4 Results

The major challenge of this set of simulations was determining the best method of comparing the maximum run-up height generated when the water column collapses for varying grain sizes. However, due to particle scattering in the MPM simulation, identifying the particle that best represents the run-up height is difficult, as demonstrated in Figure 5.3a. We could look at the highest point reached by any particle (highlighted in green), but this is obviously affected heavily by scattering. Additionally, for cases with a narrower wall, there is some reflection off the solid domain boundary, and the particles travelling back through the dam artificially increase the perceived run-up height. There is a distinct lack of certainty when viewing the simulation video and thus, results derived using this method would be challenging to defend.

Other particle combinations to identify were suggested (also depicted in Figure 5.3a): the "highest point reached by a particle in contact with the wall" (highlighted in red) or the "highest point reached by particles that are part of a continuous plume" (highlighted in orange). However, these are both subject to the same uncertainty as the above method, as they rely on the interpreter making decisions of the exact timestep and particle to select - ergo, a highly subjective and imprecise method.

Alternative methods suggested including looking at the flow front position, the pressure in the bottom left corner of the porous wall where the bubble of air as described in Hattori et al. (1994) would likely form, and the impact pressure of the wave on the wall. The main problem with all the methods proposed above are the difficulties in obtaining the relevant data, as the post-processing software (ParaView) did not necessarily give the required numbers straight out.

Due largely to the great amount of scatter at higher grain sizes and the inaccuracies presented by having to visually identify the moment of maximum run-up, it was found that the best method for comparing run-up with grain size was to take the highest centre of mass of the water wave (by averaging the y-coordinates of all the particles) during the simulation run-time. This is proportional to the run-up. Results are shown in Figure 5.2. This method is less subjective and, since there are over 20,000 particles in each simulation, any anomalous scattered particles are smoothed out.

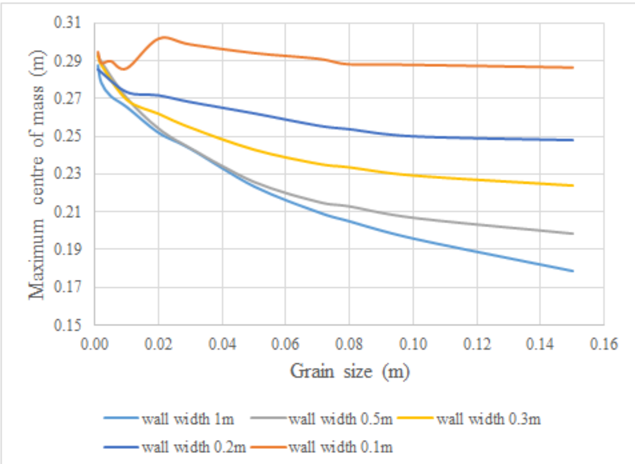

Figure 5.2: Maximum centre of mass with varying grain size

It was expected that the results would show a negative correlation, in that the run-up (represented by the maximum centre of mass) would decrease as the grain size increased - as an increased grain size means an increased porosity and thus more fluid can invade the porous dam, and a greater amount of energy is absorbed. It was also expected that the run-up would reach a value at which increasing the grain size does not affect it as the wave would be able to simple pass through as if there were no media there. Finally, the run-up at a very small grain size was expected to be the same for all wall widths and also for a non-porous domain (as in the liquid dam-break without a porous vertical seawall).

The results shown in Figure 5.2 agrees relatively well with the theorised results. However, it was observed that the centre of mass of the vertical porous seawall was much less than that of the pure liquid dam-break in a non-porous domain. This may because of the dissipation losses that occur at the soil-wave boundary interface. Also, contra to the hypothesis that more porous walls would result in lower run-up heights, Figure 5.3 shows that the run-up height is not decreasing with grain size, so there may be an issue with the method used.

As seen Figure 5.2, the run-up does reach a steady-state at a large enough grain size. This varies based on the wall width, with a wider wall having a lower steady-state run-up. This is because the maximum centre of mass for very thin walls is affected more by the reflection of liquid particles off the back of the wall than for thicker walls. Up to the steady-state, the grain size is the dominant parameter.

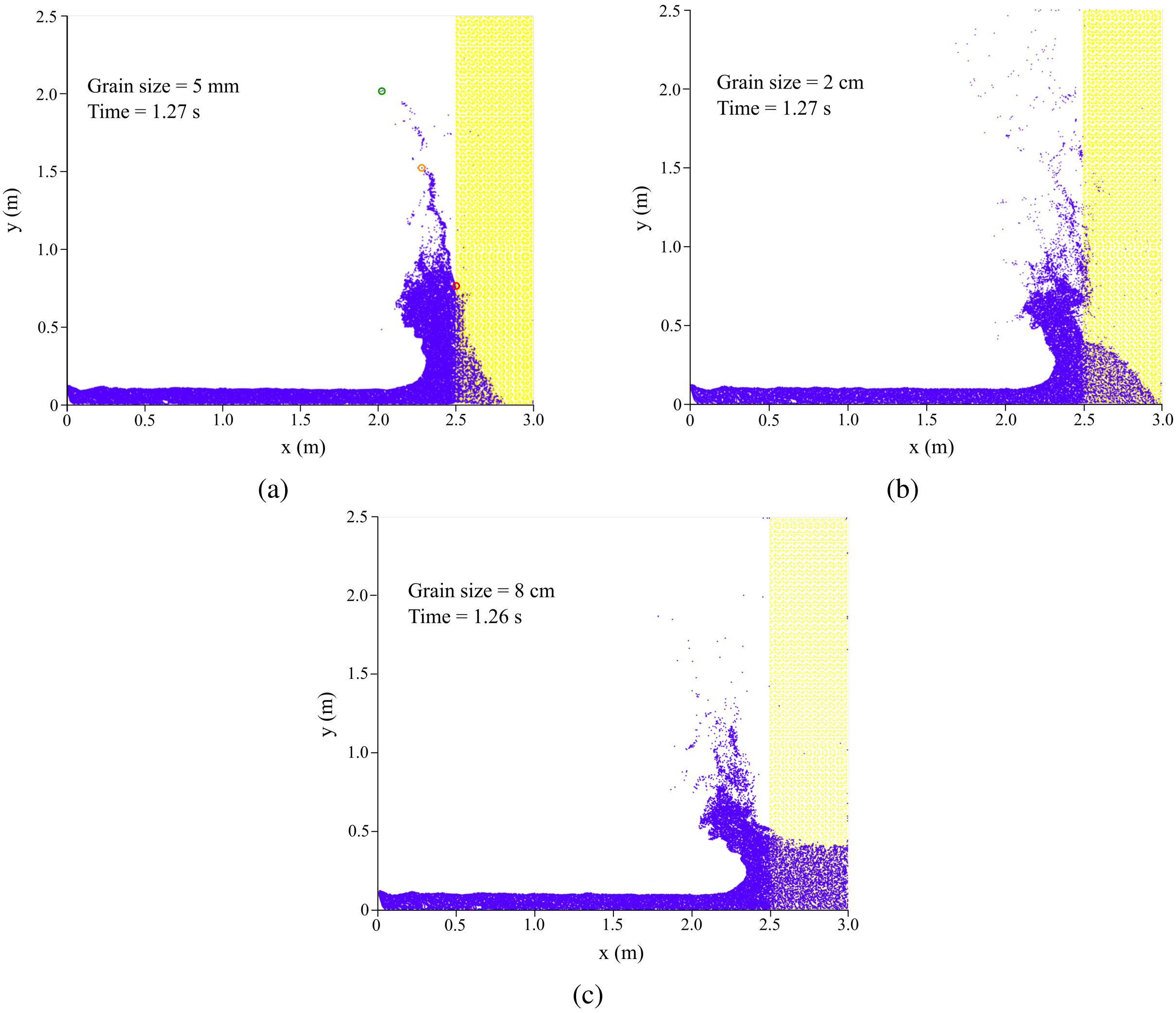

Figure 5.3: Simulation results where the run-up height based on the centre of mass appears to increase with increasing grain size D_p as a result of increased scattering (shown at point of highest centre of mass)

It was found that as the grain size increases, scattering increases notably. This scattering occurs when fluid particles reflect off the non-porous back of the porous seawall and travel back through the wall, artifically scattering and increasing the run-up height. This can be seen in the snapshots in Figure 5.3. As there is no way to reasonably determine which particles are scattered and which are not, these results are unphysical and of little interest.

In order to account for these unphysical effects, it may have been better to use a reduced volume of inspection to remove the questionable particles. Instead of taking all the liquid material points into consideration when computing the centre of mass, we would only consider particles that fall within the margin, as shown in Figure 5.4. This reduces the effect that liquid particles at the stillwater level and also any percolating liquid particles have on the centre of mass. This method may also smooth out the results that were collected and plotted in Figure 5.2.

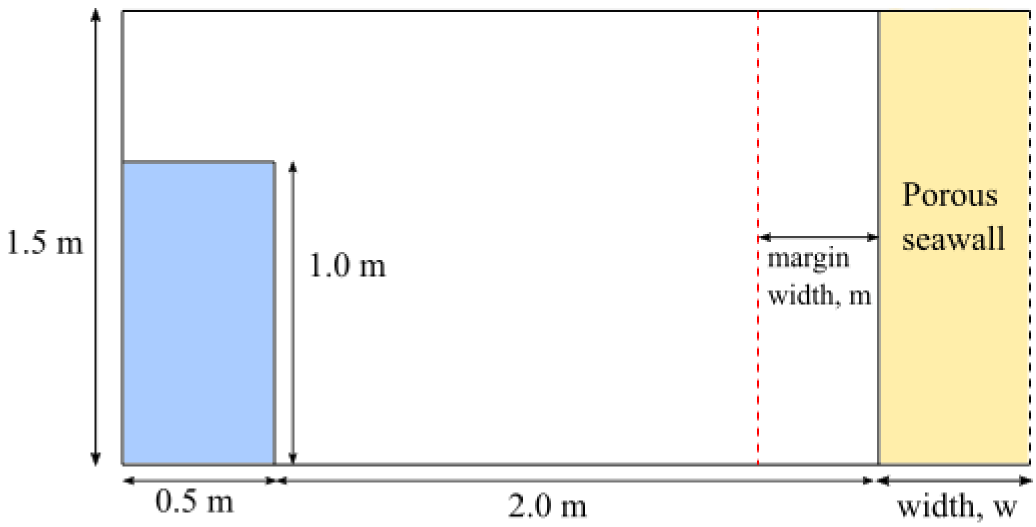

Figure 5.4: Refined run-up analysis

6 | Sloped Beach

Most of the damage associated with tsunamis is associated with their run-up on the shoreline. Upon reaching the shoreline, tsunamis can travel inland for miles, causing property damage and loss of life. Therefore it is imperative to gain a better understanding of this run-up, in order to be able to better predict the effect of any mitigation effort against sea waves.

A problem of a sloped beach has been run. Although there are a few methods to simulate a beach, the two that have been explored in depth are the column collapse and the wave generator. Another method, in which an elastic soil block is dropped on a body of water to generate a single wave, was trialled but it proved difficult to run due to meshing errors but may be worth exploring more in the future. A two-phase double-point simulation type is used; a Courant number of 0.8 is used to ensure stability.

6.1 Column collapse

6.1.1 Definition of geometry and mesh

The initial geometry is shown in Figure 6.1. The width of the porous beach layer, w, is varied and takes the values of $[0.1, 0.2, 0.3, 0.5]$ m. The liquid column has 20 fluid material points specified per element, and the soil has 4 solid material points specified per element. As the non-porous section of the beach is much less porous than the porous layer, it was not simulated at all.

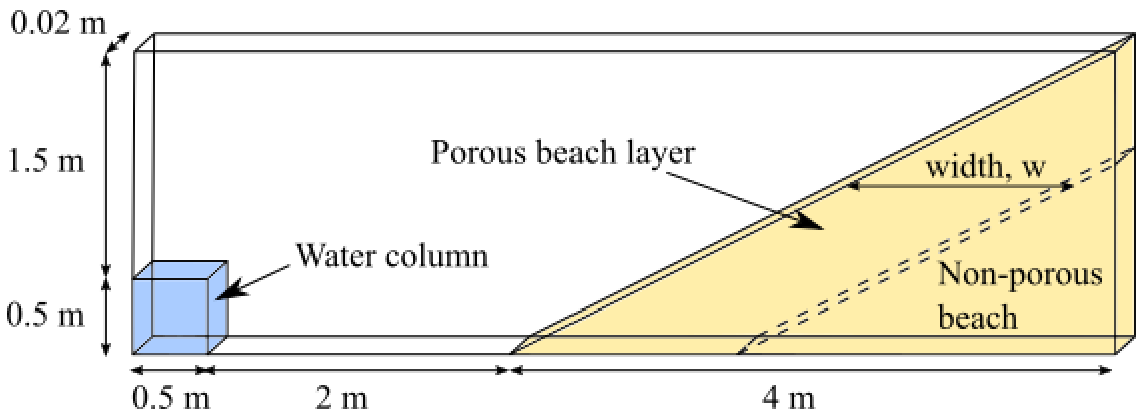

Figure 6.1: Initial geometry for sloped beach with dam-break

6.1.2 Boundary Conditions

Liquid fixities are applied to all outer boundaries of the domain, as well as at the back of the porous beach layer.

6.1.3 Material properties

The material properties for the water column are shown in Table 4.4. The properties of the beach are shown in Table 5.1.

6.1.4 Results

The results for the dam-break with the fully non-porous sloped beach are shown in Figure 6.2, with the salient time steps shown. It can be seem that the behaviour of the water is comparable to a liquid column collapse both before and after the run-up. It is interesting to note that the breaking wave in Figure 6.2h shows a similar water profile as in Liang (2009) [10] - it appears that the presence of a non-porous slope does not affect the intrinsic behaviour of the wave.

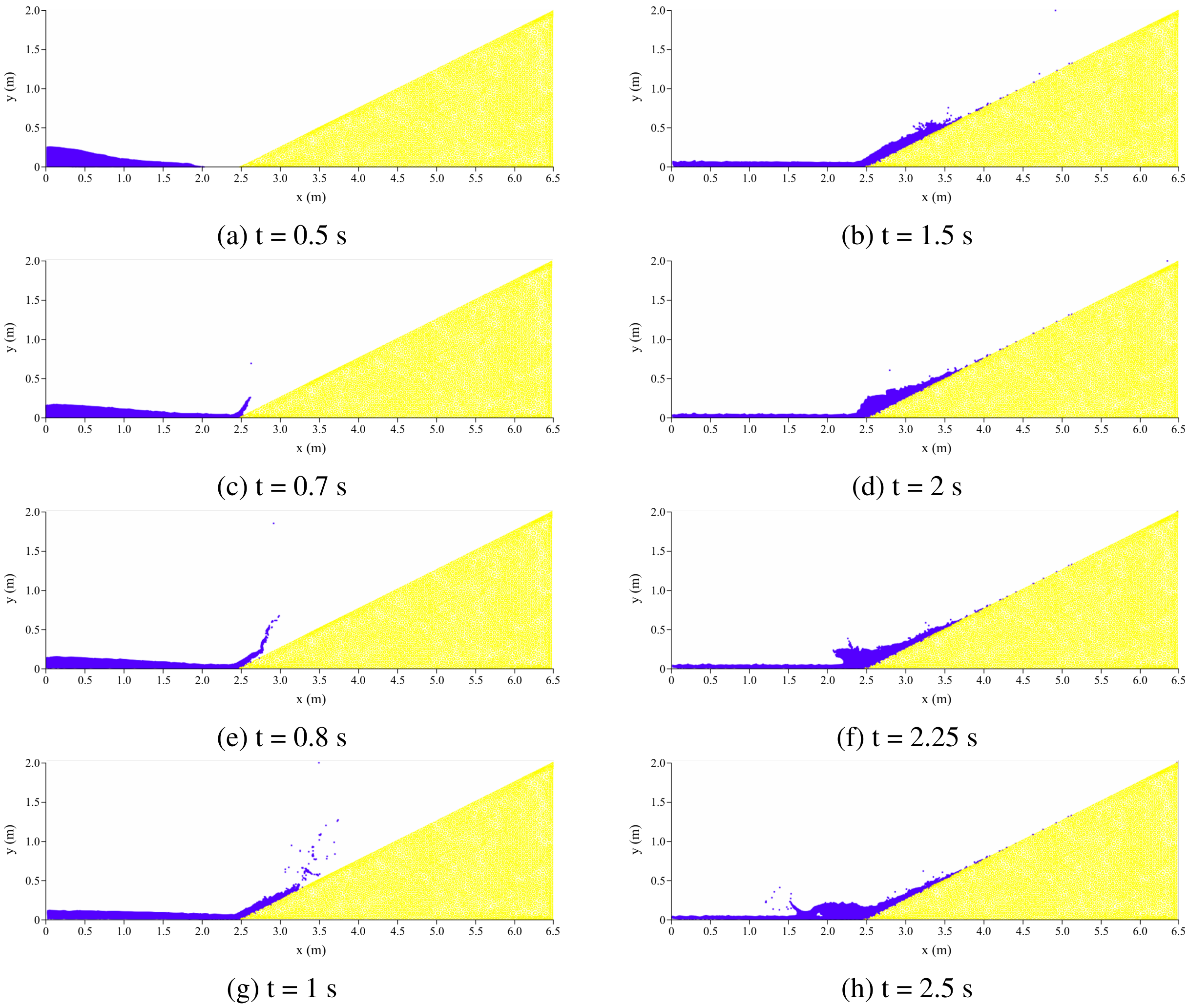

(a) t = 0.5 s (b) t = 1.5 s

(c) t = 0.7 s (d) t = 2 s

(e) t = 0.8 s (f) t = 2.25 s

(g) t = 1 s (h) t = 2.5 s

Figure 6.2: Results of a liquid dam-break from t = 0.5 s to 2.5 s

Due to the relatively large amount of scatter at some grain sizes, it was decided that the best method for this case was also to take the centre of mass to compare to the grain size. The results are shown in Figure 6.3. The expectation for these results was a similar shape and trend as shown in the vertical porous seawall case.

These results do not disappoint and show a relatively similar starting point combined with a drop to a steady-state run-up once grain size no longer has an effect. It can also be concluded that generally, that as the wall width increases, the steady-state run-up decreases for the same reasons as for the vertical seawall.

However, the one curious result is that of the porous beach width of 0.1 m. This result starts approximately 0.015 m above those of the others and decreases before increasing again. The line looks as though, given an ever increasing grain size, the run-up at large grain sizes may even surpass that at a grain size low enough to be essentially impermeable. The reason for this may be that the wall width is thin enough that it essentially acts as a non-porous slope. Another reason may be that the wall is thin enough that there is significant interaction between percolating particles and running-up particles: the particles that percolate and are reflected from the back of the porous section increase in height and lead to an increased centre of mass. It is advised that further simulations are run to test these hypotheses and also whether there is a better region of particles that could be taken into account, in a way analogous to the reduced area of consideration in the case of the vertical porous seawall.

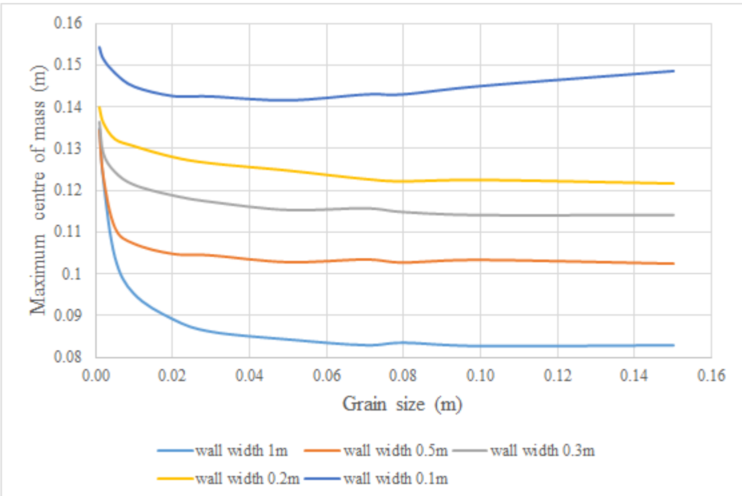

Figure 6.3: Maximum centre of mass with varying grain size for a sloped beach dam-break

6.2 Wave generator

The MPM source code was edited to allow a wave to be generated by a paddle.

6.2.1 Definition of geometry and mesh

The initial geometry used for this case is shown in Figure 6.4. The slope angle is set to 26°. The width, w, of the porous beach layer is varied from 0 m to 1 m. The full beach described in the results relates to a slope in which there is no non-porous section. Both solid and liquid have 3 material points specified per element, with the saturated soil having 3 liquid and 3 solid.

The simulations run for this case are unique in this project in that they are 2D simulations. It was deemed that a 2D simulation could be sufficiently representative of the real situation. This simulation used a triangular mesh of size 0.02 m. The maximum number of material points per element permitted was 3 for the 2D simulation, using the .exe file provided.

As the non-porous section of the beach is much less porous than the porous layer, it was not simulated at all.

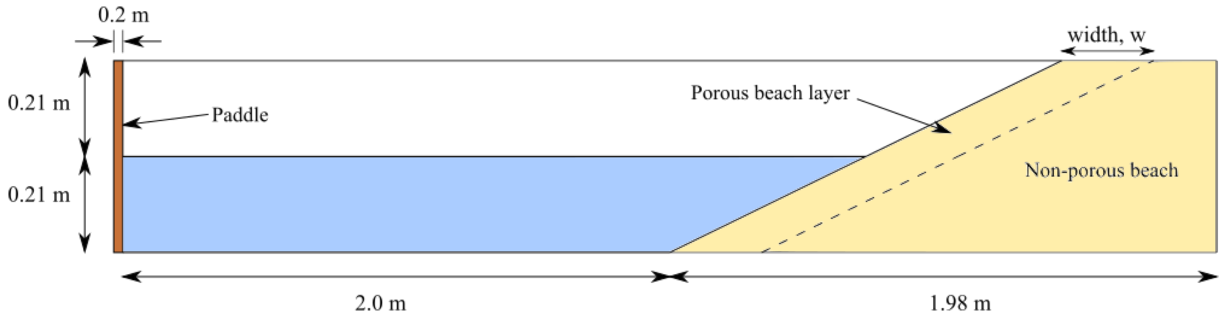

Figure 6.4: Initial geometry for sloped beach with wave generating paddle (not to scale)

6.2.2 Boundary conditions

For this case, the boundary conditions are much the same as for the sloped beach with column collapse case (as detailed in Section 6.1.2). However, there are a few differences. The main difference is that fixities are no longer surface fixities but line fixities, owing to the fact that the domain is a two-dimensional domain. A further difference is that there are no horizontal solid fixities on the leftmost paddle surface to avoid any restrictions stopping paddle movement.

6.2.3 Material properties

Table 6.1 shows the material properties of the paddle and the soil used to simulate the sloped beach. The properties of the water are as shown in Table 4.4 with the added condition of being a Newtonian liquid. In this simulation, any solid with a initial porosity of ≤ 0.42 is identified as paddle and will be given the same movement as the paddle.

Table 6.1: Material properties for wave generator simulations

material	**paddle**	**dry beach**	**saturated beach**
material type	dry material	dry material	saturated material - fully coupled
material model	Linear elasticity	Linear elasticity	Linear elasticity
initial porosity	0.42	0.43	0.43
density solid [kg/m^3]	2650	2650	2650
density liquid [kg/m^3]	-	-	1000
intrinsic permeability liquid	-	-	1e-6
bulk modulus liquid [kPa]	-	-	20000
dynamic viscosity liquid	-	-	1e-6
K_0 value [–]	0.5	0.5	0.5
Young's modulus, E [kPa]	10	10	10
Poisson's ratio [–]	0.3	0.3	0.3

6.2.4 Validation

The results obtained for the wave generator are compared with the validated results presented in Li and Raichlen (2001) [9]. This paper presents the case of a solitary wave as shown in Figure 6.5.

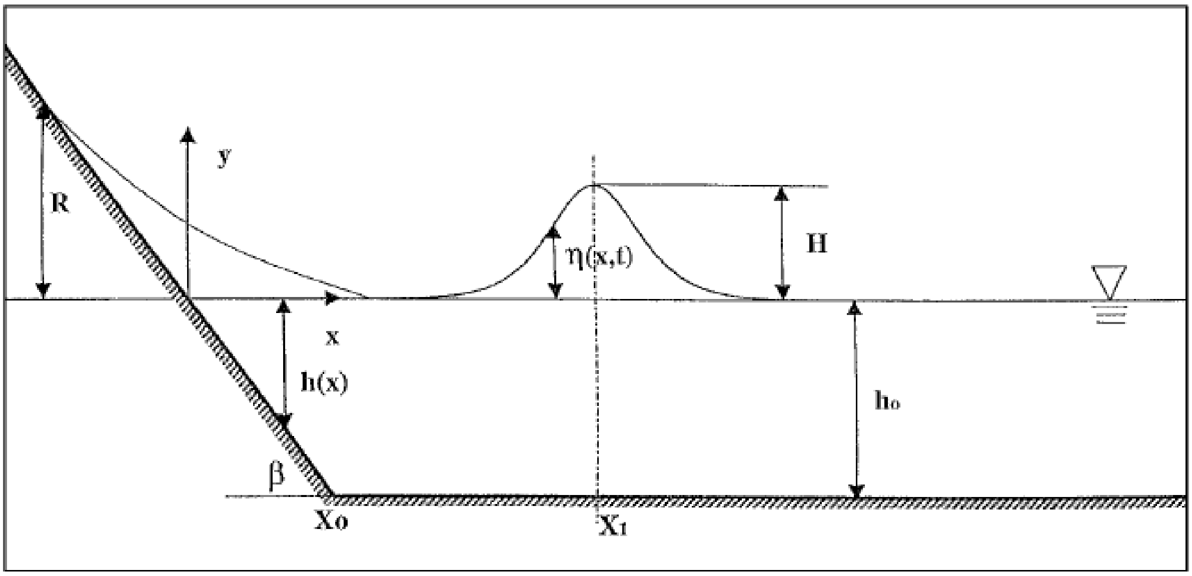

Figure 6.5: Definition sketch for solitary wave run-up from Li and Raichlen (2001) [9]

The paper also presents a formula for the maximum run-up obtained from the present non-linear theory:

$$\frac{R}{h_0} = \frac{R_s}{h_0} + \frac{R_{cr}}{h_0} = \frac{R_s}{h_0}\left(1 + \frac{R_{cr}}{R_s}\right) \tag{6.1}$$

with

$$
\begin{aligned}
\frac{R_s}{h_0} &= 2.831\sqrt{cot\beta}\left(\frac{H}{h_0}\right)^{5/4} \\
\frac{R_{cr}}{h_0} &= 0.293(cot\beta)^{3/2}\left(\frac{H}{h_0}\right)^{9/4} \\
\frac{R_{cr}}{R_s} &= 0.104cot\beta\frac{H}{h_0}
\end{aligned}
\tag{6.2}
$$

where R_s/h_0 = run-up obtained by Synolakis (1987) and R_{cr}/h_0 is the correction to the approximate theory based on the non-linear approach presented in the paper itself. Using these equations, it was found that results of the current simulation using 3 material points per element falls within 2% of the theoretical value.

The data from previous studies was also flipped (as the beach was at the left of the domain) and visually compared to the data obtained by MPM through superposition, as can be seen in Figure 6.7. In conducting this process, a new .exe file was used which allowed the number of material points per element to be increased to either 6 or 12. As such, it was possible to investigate the effect of changing the mesh size to 0.01 m as well as increasing the number of material points per element to 12. The observations were that reducing the mesh size gave more consistency than increasing the number of material points, with both coming at an additional computational cost. As such, only the results using the 3 material points per element with a reduced mesh size will be shown. The video was taken at roughly 75% of the real-time speed.

It can be seen that the MPM simulations fit very well with the previously validated data, particularly when running up the slope. Although at t = 1.8 s, the MPM results are similar to those of Li and Raichlen (2001), it quickly becomes clear that the MPM model is not apt to describe the process of the wave running down the slope in this case. This can particularly be seen at t = 2.1 s (Figure 6.7d) in which the liquid particles appear to 'stick' to the slope instead of running down. Although initially it was thought that this was due to the low number of particles meaning that a smooth surface could not be described, as can be seen in Figure 6.6, this phenomenon does not disappear with an increase in the number of MPs. More investigation is recommended to look into why this is the case and whether MPM continues to be a good numerical method for these studies.

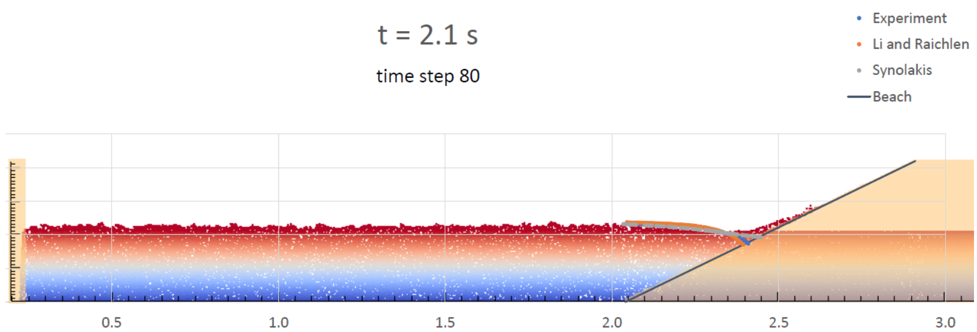

Figure 6.6: Comparison of sloped beach results with published results at t = 2.1 s for 12 MPs, mesh size = 0.02 m

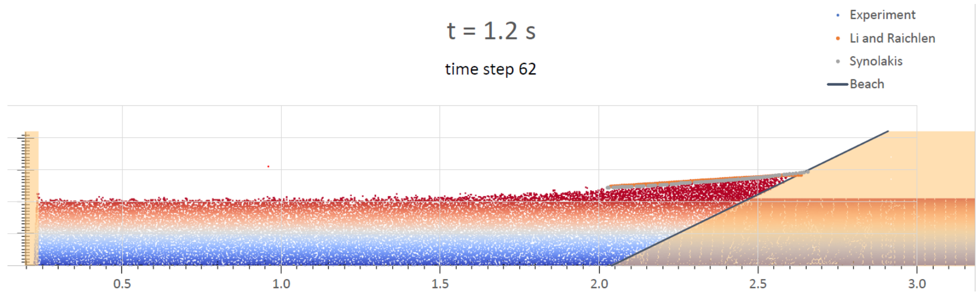

(a)

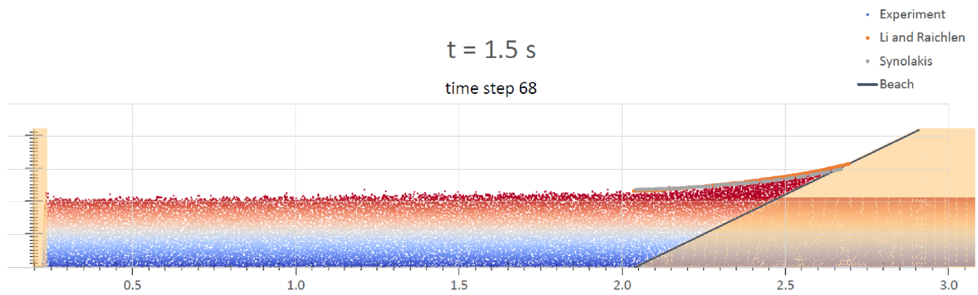

(b)

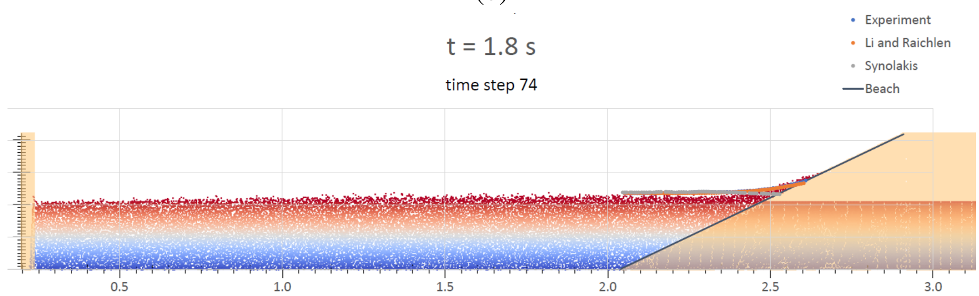

(c)

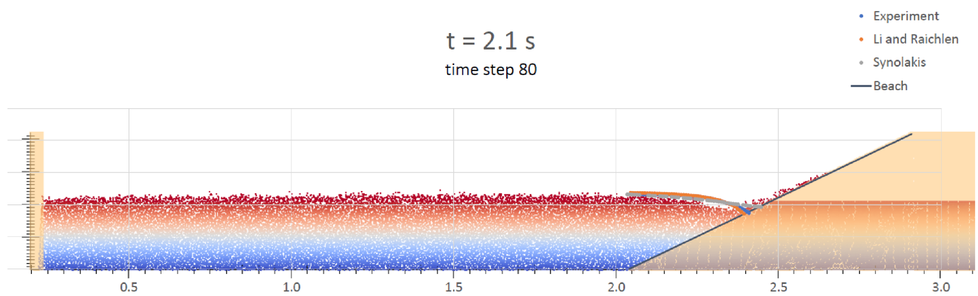

(d)

Figure 6.7: Comparison of sloped beach with wave generator results with published results at: (a) t = 1.2 s. (b) t = 1.5 s. (c) t = 1.8 s. (d) t = 2.1 s

6.2.5 Results

The previous method of measuring run-up through centre of mass was used to negate the effects of scattering particles. However, in this case, the amount of scatter is low due to the relatively shallow gradient of the beach compared to the previously used 90° for the vertical seawall. As a result, the relationship between run-up and grain size can be charted simply by finding the flow front position. This is plotted across the whole range of grain sizes investigated in Figure 6.8.

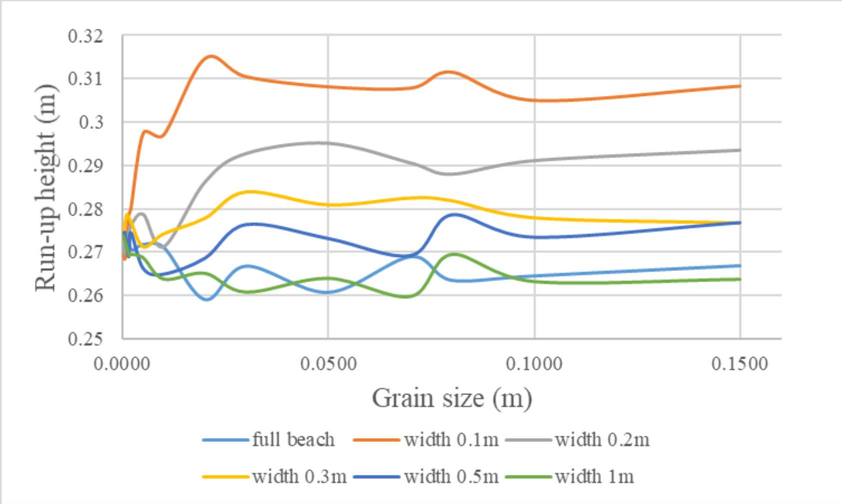

Figure 6.8: Maximum run-up with varying grain size for wave generator

It was expected that there would be a similar result as those found through using a dam-break to simulate a wave interacting with a sloped beach, as in the previous section. However, there does not appear to be an immediate relationship between the two variables. Generally, it appears that the larger the width of the beach, the lower its run-up height. Even though there are variations that appear quite large in the graph, it must be noted that these variations are only variations of approximately or less than 1 cm, which would not affect a design done with an approprate factor of safety. Through this method, it was expected that the steady-state run-up height eventually reached at a large enough grain size would simply equal the generated wave height for all wall widths. The fact that it doesn't, perhaps implies more about the water-wave interactions with the porous media that we do not yet fully understand.

Upon reflection, it was realised that many of the results used to produce Figure 6.8 were not necessary as the results for grain sizes larger than 0.002 m were too large and simply allowed the wave to pass straight through the beach, reflect off the back and pass straight back through again. Figure 6.9 shows the results for grain sizes between 0.1 mm and 2 mm. The lower bound of these grain sizes was taken as this is the smallest grain size before which the soil is considered a clay. At 0.1 mm, it appears that all of the wall widths produce very similar run-up heights - and thus, one can conclude that at this grain size, the porous beach acts very much like a non-porous wall. Moving up the grain sizes from 0.1 mm to 2 mm, it appears that the data continues to not follow a trend. It is interesting to note, however, that when viewed on a semi-log plot, there is little variation in the results until very close to 0.001 m, when the results start to diverge, which is more easily visualised on a semi-log graph in which the grain size axis is logarithmic. Even looking at the results in Figure 6.9, the variation between various wall widths is at most about 1 cm. This is small and, in terms of design, would not have too much of an impact given the larger factors of safety that would be used in areas with a high probability of flooding.

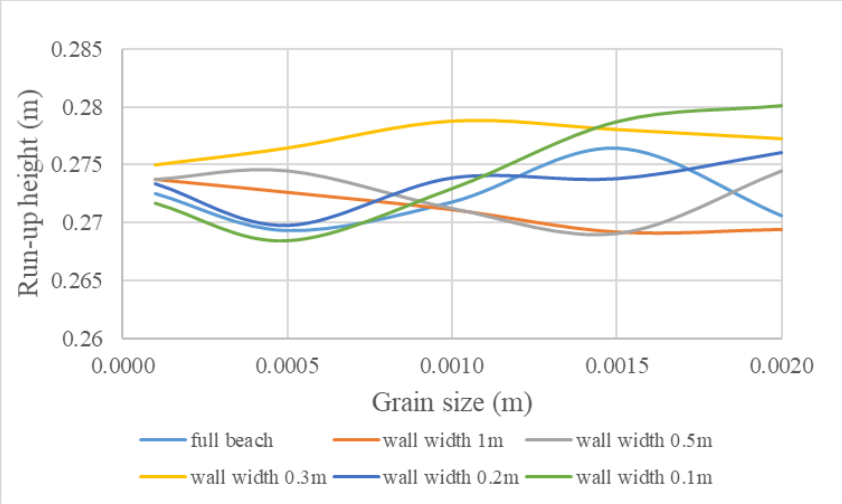

Figure 6.9: Maximum run-up with varying grain size (0.1 mm < d < 2 mm) for wave generator

To be consistent with the results obtained from the sloped beach with dam-break, results were also taken using the centre of mass method. However, unlike the previous use of this method, only particles above the stillwater level (i.e. 0.21 m above the bed) are taken into account as this gives a result more comparable to those taken above. The results for the full range of grain sizes tested were very similar to those obtained from the flow front position method and plotted in Figure 6.8.

The results for grain sizes between 0.01 mm and 2 mm are much more interesting, however. It is interested to note the downwards trend that is apparent in this method that is not seen in the flow front position method results. The results also seem to follow a more similar pattern, than they did in Figure 6.9, thus the results are more consistent. The differences in the largest and smallest results are all smaller too, with the largest appearing at 2 mm, being approximately 3 mm. It is highly recommended that a continuation of the study be carried out as the results, though generated have yet to be analysed in any way which yields definitive results.

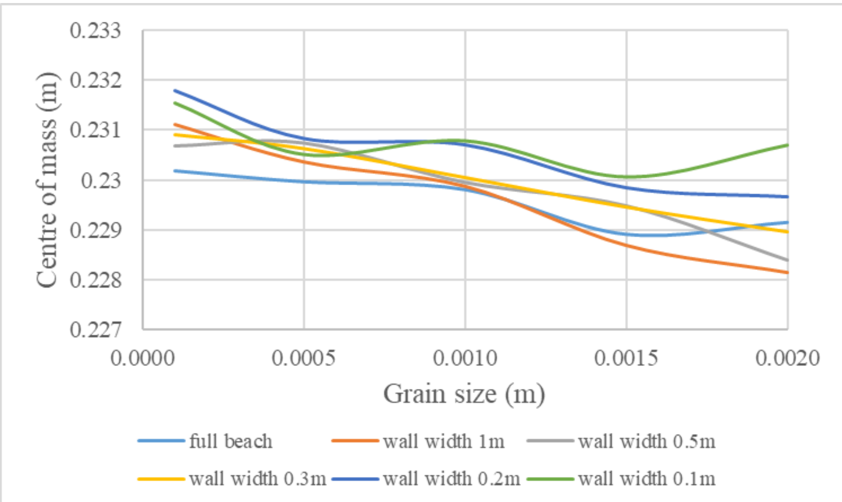

Figure 6.10: Maximum centre of mass for particles above 0.21 m with varying grain size for 0.01 mm < d < 2 mm

7 | Conclusions

During the course of this project, the concept and implementation of the MPM were reviewed. It was found that MPM is a robust numerical computational method which can be used to model the complex water-soil interactions that are required to investigate the effect of water-waves on porous media.

It was also observed that, generally, increasing the grain size of a porous layer in a porous coastal structure decreases the run-up. At a large enough grain size, the run-up is independent of grain size and is only affected by the porous layer width.

To further the work done on the sloped beach, it would be pertinent to investigate the relationship between grain size and run-up with different slope angles, once more definitive relationships have been found between the variables at the current slope of 26°. In the future, the paddle could also be programmed to generate multiple waves, to better simulate the normal behaviour of sea waves, rather than tsunami waves.

The literature implies that the effects of turbulence must be accounted for in order to achieve realistic results. As such, a suitable step following completion of the sloped beach analysis may be to find a way of incorporating turbulence into the MPM model.

Bibliography

[1] BRACKBILL, J. U., KOTHE, D. B., AND RUPPEL, H. M. FLIP: a low-dissipation, particle-in-cell method for fluid flow. *Computer Physics Communications* (1988), 48(1):25–38.

[2] BULLOCK, G., OBHRAI, C., PEREGRINE, D., AND BREDMOSE, H. Violent breaking wave impacts. Part 1: Results from large-scale regular wave tests on vertical and sloping walls. *Coastal Engineering* (2007), 54(8):602–617.

[3] FERN, E., AND SOGA, K. The role of constitutive models in MPM simulations of granular column collapses. *Acta Geotechnica* (2016), 11(3):659–678.

[4] HATTORI, M., ARAMI, A., AND YUI, T. Wave impact pressure on vertical walls under breaking waves of various types. *Coastal Engineering* (1994), 22:79–114.

[5] HIRT, C. W., AND NICHOLS, B. D. Volume of fluid (VOF) method for the dynamics of free boundaries. *Journal of Computational Physics* (1981), 39(1):201–225.

[6] HUANG, L., AND CHAO, H. Reflection and transmission of water wave by porous breakwater. *Journal of Waterway, Port, Coastal and Ocean Engineering* (1992), 118(5):437–452.

[7] KORAIM, A., HEIKAL, E., AND ZAID, A. A. Hydrodynamic characteristics of porous seawall protected by submerged breakwater. *Applied Ocean Research* (2014), 46:1–14.

[8] LEAN, G. H. A simplified theory of permeable wave absorbers. *Journal of Hydraulic Research* (1967), 5(1):15–30.

[9] LI, Y., AND RAICHLEN, F. Solitary wave runup on plane slopes. *Journal of Waterway, Port, Coastal and Ocean* (2001), 127:33–44.

[10] LIANG, D. Evaluating shallow water assumptions in dam-break flows. *Proceedings of the Institution of Civil Engineers - Water Management* (2009), 163:227–237.

[11] LIANG, D. Evaluating shallow water assumptions in dam-break flows. *Proceedings of the Institution of Civil Engineers - Water Management* (2010), 163(5):227–237.

[12] LIU, P.-F., LIN, P., CHANG, K.-A., AND SAKAKIYAMA, T. Numerical modeling of wave interaction with porous structures. *Journal of Waterway, Port, Coastal and Ocean Engineering* (1999), 125(6):322–330.

[13] Martin, J. C., and Moyce, W. J. An experimental study of the collapse of liquid columns on a rigid horizontal plane. *Philosophical Transactions of the Royal Society of London Series A* (1952), 244(88):312–324.

[14] NOAA (National Oceanic and Atmospheric Administration). Global and regional sea level rise scenarios for the United States. *NOAA Technical Report NOS CO-OPS 083* (January 2017).

[15] Ogolo, N., Akinboro, O., Inam, J., A. F., and Onyekonwu, M. Effect of grain size on porosity revisited. *SPE Nigeria Annual International Conference and Exhibition* (2015).

[16] Sakakiyama, T., and Liu, P. L. F. Laboratory experiments for wave motions and turbulence flows in front of a breakwater. *Coastal Engineering* (2001), 117–139.

[17] Savage, R. P., and Fairchild, J. C. Laboratory study of wave energy losses by bottom friction and percolation. *Coastal Engineering Research Centre, Vicksburg* (1953).

[18] Straub, L., Bowers, C., and Herbich, J. Laboratory studies of permeable wave absorbers. *Proceedings of 6th Conference on Coastal Engineering* (1957), 729–742.

[19] Sulisz, W. Wave reflection and transmission at permeable breakwaters of arbitrary cross-section. *Coastal Engineering* (1985), 9(4):371–386.

[20] Sulsky, D., Chen, Z., and Schreyer, H. A particle method for history-dependent materials. *Computer Methods in Applied Mechanics and Engineering* (September 1994), 118:179–196.

[21] Sulsky, D., Zhou, S.-J., and L. Schreyer, H. Application of particle-in-cell method to solid mechanics. *Computer Physics Communications 87* (1995), 236–252.

[22] Zhao, X., and Liang, D. MPM modelling of seepage flow through embankments. *International Society of Offshore and Polar Engineers* (June 2016).

[23] Zhao, X., Liang, D., and Martinelli, M. MPM simulations of dam-break floods. *Journal of Hydrodynamics, Ser. B* (2017), 29(3):397–404.

A | Risk assessment

The risk assessment submitted to the Safety Office at the start of Michaelmas term 2018 is attached below. In retrospect, the form accurately reflects the hazards encountered during the project. As this was a project based on running computer simulations, the risks would likely not have been evaluated differently if starting the project again.

More care should be taken with the use of the guidance on working with display screen equipment.